Interactions of the Human Calcitonin Fragment 9–32 with Phospholipids: A Monolayer Study

Kerstin Wagner,*† Nicole Van Mau,* Sylvie Boichot,‡ Andrey V. Kajava,* Ulrike Krauss,† Christian Le Grimellec,‡ Annette Beck-Sickinger,† and Frédéric Heitz*

*Centre de Recherches de Biochimie Macromoléculaire-Centre National de la Recherche Scientifique, Formation de Recherche en Evolution 2593, F-34293 Montpellier Cedex, France; †Institute of Biochemistry, University of Leipzig, D-04103 Leipzig, Germany; and ‡Nanostructures et Complexes Membranaires, Centre de Biologie Structurale Institut National de la Santé et de la Recherche Medicale U554, F-34090 Montpellier Cedex, France

ABSTRACT Human calcitonin and its C-terminal fragment 9–32 (hCT(9–32)) administered in a spray translocate into respiratory nasal epithelium with an effect similar to intravenous injection. hCT(9–32) is an efficient carrier to transfer the green fluorescent protein into excised bovine nasal mucosa. To understand the translocation of hCT(9–32) across plasma membranes, we investigated its interactions with phospholipids and its interfacial structure using model lipid monolayers. A combination of physicochemical methods was applied including surface tension measurements on adsorbed and spread monolayers at the air-water interface, Fourier transform infrared, circular dichroism, and atomic force microscopy on Langmuir-Blodgett monolayers. The results disclose that hCT(9–32) preferentially interacts with negatively charged phospholipids and does not insert spontaneously into lipid monolayers. This supports a nonreceptor-mediated endocytic internalization pathway as previously suggested. Structural studies revealed a random coil conformation of hCT(9–32) in solution, transforming to α-helices when the peptide is localized at lipid-free or lipid-containing air-water interfaces. Atomic force microscopy studies of monolayers of the peptide alone or mixed with dioleoylphosphatidylcholine revealed that hCT(9–32) forms filaments rolled into spirals. In contrast, when interacting with dioleoylphosphatidylglycerol, hCT(9–32) does not adopt filamentous structures. A molecular model and packing is proposed for the spiral-forming hCT(9–32).

INTRODUCTION

Human calcitonin (hCT) is a 32 amino acid peptide hormone, present in the thyroid of vertebrates, which has an important role in calcium metabolism and possesses a number of other biological activities (Nakamuta et al., 1990; Colman et al., 2002). The hypocalcemic effect has been correlated with the binding of hCT to different types of receptors depending on the conformational state of the calcitonin molecule (Nakamuta et al., 1991). Using chimeric receptors that bind salmon calcitonin (sCT), Stroop et al. (1996) showed that the helical part has a binding site whereas the conserved N-terminal part is essential for receptor activation. Previous studies have also shown that hCT penetrates in respiratory nasal epithelium as efficiently when administrated by spray as by intravenous injection (Silverman, 1997). A nonreceptor mediated endocytic internalization pathway was proposed since the translocation of hCT and its C-terminal fragment hCT(9–32) through excised bovine nasal mucosa was shown to be associated with vesicular internalization (Schmidt et al., 1998). Moreover, the C-terminal fragment of hCT was used as a carrier to transport efficiently the green fluorescent protein into excised bovine nasal mucosa (Machova et al., 2002). Finally, sCT and hCT were also shown to induce formation of voltage-dependent channels that permeate calcium through lipid bilayers (Stipani et al., 2001).

Taken together, these investigations favor the idea that hCT translocates through membranes, but the mechanism of this translocation through lipidic plasma membranes is still unknown. Therefore, we investigated the interactions of hCT(9–32), the most efficient cell-penetrating shortened hCT analog obtained so far (Schmidt et al., 1998), with phospholipids using the monolayer approach. This membrane model has several advantages as it can provide information about the conformational state(s) of the carrier peptide in an interfacial situation similar to that occurring in membranes. Furthermore, such an approach allows the analysis of the peptide-lipid interactions under controlled parameters, mainly lateral pressure and lipidic composition (Brockman, 1999). Therefore, this approach can provide information about the transfer across membranes and thus about the first step of the cellular internalization. In this work, we studied, first, the ability of the peptide to insert into lipid monolayers of different composition, and second, the interactions that could occur between the peptide and various types of lipids as well as the consequences of these interactions on the peptide structure together with the lateral organization of both components, and propose a model for the peptide arrangement.

MATERIALS AND METHODS

Materials

9-Fluorenylmethyloxycarbonyl (Fmoc)-protected amino acids, 1-hydroxybenzotriazole and 4-(2′,4′-dimethoxyphenyl-Fmoc-aminomethyl)phenoxy

Submitted November 4, 2003, and accepted for publication March 26, 2004.

Address reprint requests to Frédéric Heitz, E-mail: heitz@crbm.cnrs-mop.fr; Annette Beck-Sickinger, E-mail: beck-sickinger@uni-leipzig.de; or Christian Le Grimellec, E-mail: clg@cbs.univ-montp1.fr.

0006-3495/04/07/386/10 $2.00

doi: 10.1529/biophysj.103.036921

resin were obtained from Novabiochem (Bad Soden, Germany), diisopropylcarbodiimide from Sigma-Aldrich (Buchs, Switzerland), and trifluoroacetic acid (TFA, peptide synthesis grade) from Riedel-de Haen (Seelze, Germany). Piperidine, thioanisole, *p*-thiocresol, and trifluoroacetic acid (HPLC grade) were purchased from Fluka (Buchs, Switzerland). *N*,*N*-dimethylformamide and diethyl ether were from Biosolve (Valkenswaard, The Netherlands), acetonitrile (ACN) was from Merck (Darmstadt, Germany), and phosphate buffer saline (PBS) from Invitrogen (Carlsbad, CA).

Phospholipids

Dioleoylphosphatidylcholine (DOPC), dioleoylphosphatidylglycerol (DOPG), dipalmitoylphosphatidylcholine (DPPC), and dipalmitoylphosphatidylglycerol (DPPG) were purchased from Avanti Polar Lipids (Alabaster, AL). Natural erythrocytes bovine sphingomyelin (SM), monosialoganglioside (G_{M3}), synthetic Lα-phosphatidylcholine-β-palmitoyl-γ-oleoyl (POPC), and cholesterol (Chol) were from Sigma (St Louis, MO). The solvents chloroform and methanol were from Merck.

Peptide synthesis

The peptide fragment 9–32 of human calcitonin, the sequence of which is $L^{9}GTYTQDF^{16}NKFHTFP^{23}QTAIGVGAP^{32}$-$NH_2$, was synthesized by automated multiple solid-phase peptide synthesis (Fmoc strategy) using a robot system (Syro, MultiSynTech, Bochum, Germany). To obtain the peptide amide, 4-(2′,4′-dimethoxyphenyl-Fmoc-aminomethyl)phenoxy (rink amide) resin was used. The polymer matrix was polystyrene-1%-divinylbenzene (30 mg, 15 μmol). The side-chain protections were chosen as follows: Tyr (*tert*-butyl), Thr (*tert*-butyl), His (trityl), Gln (trityl), Asn (trityl), Asp (OtBu), and Lys (*tert*-butyloxycarbonyl). Double coupling procedures were carried out with diisopropylcarbodiimide/1-hydroxybenzotriazole activation, 10-fold excess, and a coupling time of 40 min. The Fmoc group was removed with 40% piperidine in *N*,*N*-dimethylformamide for 3 min, followed by 20% piperidine for 7 min. The peptide amide was cleaved with 1 mL of trifluoroacetic acid/thioanisole/thiocresol (90:5:5 v/v/v) within 3 h. The peptide was precipitated from cold diethyl ether, collected by centrifugation, and lyophilized from water/ACN (9:1 v/v). The peptide was analyzed by high-performance liquid chromatography using a LiChrospher 100 RP-18 column (linear gradient from 10–60% *B* in *A* over 30 min; $A = 0.1\%$ TFA in water, $B = 0.08\%$ TFA in ACN) and matrix-assisted laser desorption ionization mass spectrometry. Correct mass was found at 2610.0 (calculated, 2608.3); purity according to high-performance liquid chromatography was >96%.

Fourier transform infrared spectroscopy

Fourier transform infrared (FTIR) spectroscopy spectra were obtained on a Bruker (Wissembourg, France) IFS 28 spectrometer equipped with a liquid nitrogen cooled mercury-cadmium-tellurium detector. The spectra (1000–2000 scans) were recorded at a spectral resolution of 4 cm^{-1} and were analyzed using the OPUS/IR2 program. They were recorded with samples that had been obtained by deposition of solutions of lipid-peptide mixtures on a calcium fluoride plate from which the solvents were allowed to evaporate under a nitrogen flux.

Circular dichroism measurements

Circular dichroism (CD) spectra were recorded on a Jasco 810 (Jasco, Tokyo, Japan) dichrograph using quartz cells with an optical path of 1 mm for peptide in aqueous solutions. For samples transferred by the Langmuir-Blodgett (LB) method, quartz plates were used and eight plates were collected to amplify the detected signal. The band positions were determined after smoothing the spectra by the method of Savitzky and Golay (1964). The experiments were repeated twice, giving identical results within 10%.

Adsorption at the air-water interface

Adsorption studies at the air-water interface were carried out using a MicroTrough S and analyzed with the FilmWare 2.41 program, both from Kibron (Helsinki, Finland). Measurements were made at equilibrium after the injection of aliquots of an aqueous solution of the peptide into the aqueous subphase, which was gently stirred using a magnetic stirrer. To determine the critical micellar concentration (CMC), this procedure was repeated until no further increase of the surface pressure could be detected.

Penetration into lipid monolayers

For measurements of the penetration of the peptide into phospholipids, a lipid monolayer was obtained initially by spreading a solution of the lipid in chloroform/methanol (3:1, v/v) on the air-PBS aqueous solution interface to ensure a definite surface pressure. The solvent was then allowed to evaporate, and when a constant surface pressure was reached, a small volume of the aqueous peptide solution was injected into the subphase beneath the lipid monolayer. Increases of surface pressure were recorded for different initial lipid surface pressures to determine the critical pressure of insertion (CPI) of the peptide into lipids.

Peptide-lipid interactions: monolayer compression isotherms

Compression isotherms of mixed peptide-lipid monolayers were recorded using a Langmuir balance setup with a 657 cm^2 Teflon trough. Surface tensions were measured with a Prolabo (Paris, France) tensiometer based on the Wilhelmy (Adamson, 1990) method using a platinum plate as previously described. Isotherms were recorded on an XY recorder (model BD 91) from Kipp and Zonen (Delft, The Netherlands). Lipid-peptide mixtures were dissolved in a DMSO/chloroform/methanol mixture 0.01:1:3 (v/v/v); the solvent was allowed to evaporate at least 5 min before compression, which was carried out at a rate of 0.015 nm^2/molecule/min.

Langmuir-Blodgett transfer monolayers

All transfers were carried out on appropriate and wettable solid supports (quartz slides for CD and freshly cleaved mica for atomic force microscopy (AFM)) using a homemade setup with a procedure previously described (Van Mau et al., 1999; Vié et al., 2000). During the LB transfers, the surface pressure was maintained constant through a feedback system. The selected surface pressure was 20 mN/m, a value close to that of the collapse pressure of pure hCT(9–32).

Atomic force microscopy observations on transferred monolayers

The AFM observations of the LB films were performed as previously described (Vié et al., 2000) in the contact mode under ambient conditions on a Nanoscope IIIA (Digital Instruments, Santa Barbara, CA) equipped with a J scanner. Topographic images were acquired in constant-force mode using silicon nitride tips on cantilevers with a nominal spring constant of 0.1 N/m, at a scan rate of 1 Hz. Typically, the estimated imaging forces were below 1 nN. Images were obtained from at least two different samples for each condition. Representative images are presented below in Figs. 7–9. Transfers were achieved within 30 min after spreading at the interface.

Molecular modeling

The initial template for a structural model of hCT(9–32) was taken from the crystal structure of the bovine heart cytochrome C oxidase (Yoshikawa et al.,

1998). A fragment A186–A209 of this structure represents a typical α-helix with a bend produced by a proline residue. The Homology module of the INSIGHT II package (Dayring et al., 1986) was used to modify the amino acids of the template in accordance with the sequence of hCT(9–32). Then the structure was refined by the energy minimization procedure, based on the steepest descent algorithm (300 steps) implemented in the Discovery subroutine of INSIGHT II. The axial orientation of the amphipathic α-helices in the layer was chosen with the assumption that hydrophobic patches of the α-helices compose one surface of the layer whereas hydrophilic domains form another surface of the layer. Such an orientation was selected manually using the INSIGHT II package (Dayring et al., 1986). The N-terminal parts of the α-helices were positioned in-register to allow a favorable knob-in-hole packing of the side chain between the helices. Before the energy minimization of such a layer, the interhelical distance was selected at 1.15 nm and conformations of several side chains that are involved in the interhelical packing was changed by manual variation of the torsion angles to remove sterical tension. The layer that contains four identical α-helices was refined by the energy minimization procedure, based on the steepest descent algorithm (300 steps). The final stage of minimization was 1000 steps of the conjugate gradients algorithm to a root mean-square derivative of 0.3 kcal·mol^{-1}·Å^{-1}. The consistent valence force field (Dauber-Osguthorpe et al., 1988) was used for the energy calculations. The calculations were carried out in vacuum. To generate a long regular layer containing identical α-helices with uniform interhelical distances, one of the internal α-helices and a typical interhelical arrangement were chosen from the minimized four-helical layer. The program PROCHECK (Laskowski et al., 1993) was used to check the quality of the modeled structure. Images of the molecular structures on Fig. 10 were generated by the INSIGHT II package.

RESULTS AND DISCUSSION

Adsorption at the air-water interface

Before investigating the adsorption of hCT(9–32) at lipid-containing air-water interfaces, we first determined the peptide concentration required to carry out this type of experiment. Such a concentration corresponds to that which generates the maximum effect on the surface tension of a lipid-free air-water interface. For this purpose, hCT(9–32) was allowed to adsorb at the air-water interface and the surface pressure was measured upon increasing the peptide concentration in the subphase. Fig. 1 shows the variation of the surface pressure (Π) as a function of the peptide concentration (C) and reveals a sigmoidal shape similar to that already observed for amphiphilic peptides (Maget-Dana et al., 1999). A strong increase of the surface pressure $\sim 2.10^{-7}$ Mole/L and a saturation at 15 mN/m that occurs at $\sim 2.5.10^{-7}$ Mole/L can be observed. This behavior confirms the strong amphipathic character of the peptide hCT(9–32) and its ability to aggregate with formation of micelles above a concentration of $\sim 2.5.10^{-7}$ Mole/L. When no PBS is present in the subphase, saturation occurs at 11 mN/m. The surface pressure increase upon the addition of ions in the subphase can very probably be assigned to the increase in hydrophobic interactions. Taking into account the above results and the observations that full length sCT adsorbs on solid surfaces and has a strong tendency to aggregate when in solution (Law and Shih, 1999), we emphasize that the storage of calcitonin solutions has to be made carefully to prevent artifacts arising from aggregation and/or a loss of material by adsorption on the glass containers.

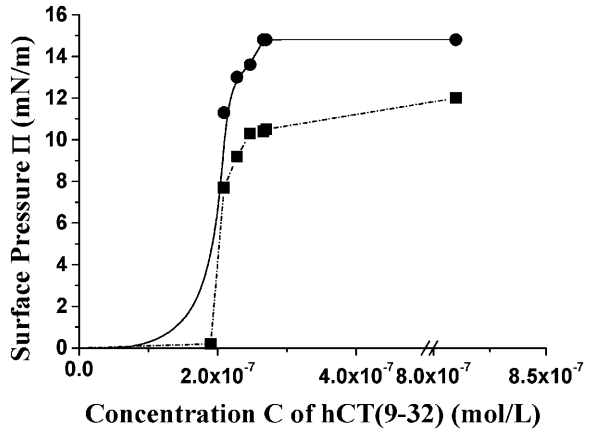

FIGURE 1 Concentration dependence of the adsorption of hCT(9–32) at the air-water (■) and air-phosphate saline buffer (●) interface.

On the basis of the Π-C variation reported above, all further experiments dealing with phospholipids were carried out using a peptide concentration close to its CMC, i.e., $2.5.10^{-7}$ Mole/L.

Penetration into lipid monolayers

Since neutral phosphatidylcholine has been shown to be the most abundant in olfactory mucosa, penetration experiments were first carried out with phospholipids bearing this type of headgroup. Monolayers made of pure DOPC, DPPC, or POPC, as well as for a 1:1 (mol/mol) mixture of DOPC/DPPC, led to very similar adsorption patterns (Fig. 2 *A*) with a critical pressure of insertion, i.e., the pressure above which the peptide cannot insert into a monolayer (CPI) of $\sim$14 mN/m and an extrapolation of the maximum pressure increase, i.e., no lipid at the interface at 14 mN/m, which is close to the experimental value obtained in the absence of lipid (see Fig. 1).

To examine the effect of negatively charged headgroups, these experiments were repeated using lipids bearing the phosphoglycerol headgroup, namely DOPG, DPPG, and a 1:1 (mol/mol) mixture of both lipids. For all three situations, the variations of Π as a function of the initial pressure (Π_i) are again almost superimposable (Fig. 2 *B*) with an average CPI of 15.5 mN/m.

To check the influence of other constituents that are often present in plasma membranes, we investigated the possible role of SM and of the glycosphingolipid G_{M3}, which are known to act as cell surface receptors. For POPC/SM and POPC/G_{M3} 1:1 (mol/mol) mixtures with and without cholesterol, a fluidity modifier component present in all plasma membranes, the CPI is $\sim$17 mN/m (Fig. 2 *C*), which is in the same range as the CPI found with negatively charged phospholipids. Since all critical pressures of insertion are far below the lateral pressure expected for a cell membrane

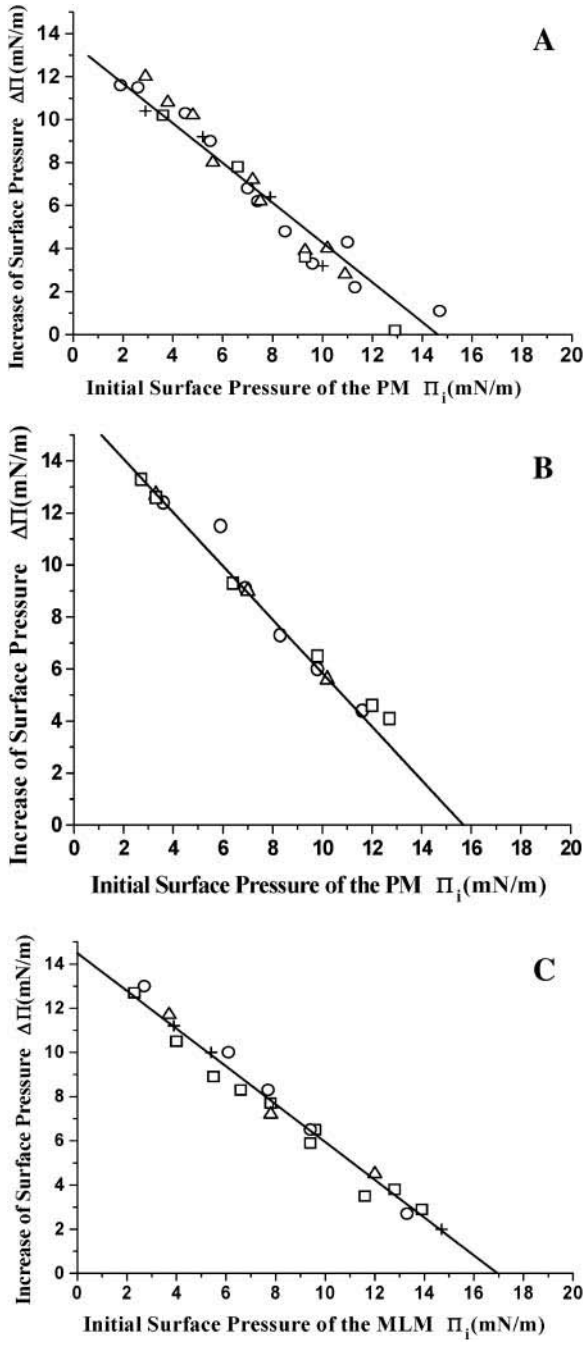

FIGURE 2 Variations of the surface pressure ($\triangle\Pi$) as a function of the initial pressure of the phospholipid monolayer. The peptide hCT(9–32) concentration in the PBS-containing subphase was 0.3 μM. (*A*) ○, DOPC; △, DPPC; □, DOPC/DPPC 1:1 (mol/mol); and +, POPC. The straight line corresponds to the linear fit of the data obtained with DOPC, and the intercept with the axis of the initial pressure leads to the critical pressure of insertion (CPI). (*B*) ○, DOPG; △, DPPG; and □, DOPG/DPPG 1:1 (mol/mol). The straight line corresponds to the linear fit of the data obtained with DOPG and the intercept with the axis of the initial pressure leads to the CPI. (*C*) □, POPC/SM 1:1 (mol/mol); ○, POPC/SM/Chol 1:1:0.4 (mol/mol); +, POPC/G_{M3} 1:1 (mol/mol); and △, POPC/GM3/Chol 1:1:0.4 (mol/mol). The straight line corresponds to the linear fit of the data obtained with POPC/SM and the intercept with the axis of the initial pressure leads to the CPI.

(≈35 mN/m) (Demel et al., 1975), it can be concluded that at concentrations up to the CMC, the peptide hCT(9–32) cannot insert spontaneously into lipidic bilayers that are devoid of any further component that would act as receptor. This conclusion is in full agreement with the model proposed by Stroop et al. (1996) in which the interaction of full-length hCT with the transmembrane receptor occurs through the N-terminal domain, which is lacking in our case.

Peptide-lipid interactions: monolayer compression isotherms

To identify the nature of the lipid-peptide interactions, we spread mixtures of the components at different peptide molar fractions with various lipids on an aqueous subphase. The compression isotherms obtained with DOPC and DOPG are shown in Fig. 3, *A* and *B*, respectively; the corresponding variations of the mean molecular area as a function of the peptide molar fraction at a constant surface pressure of 16 mN/m are reported in Fig. 4, *A* and *B*. Examination of

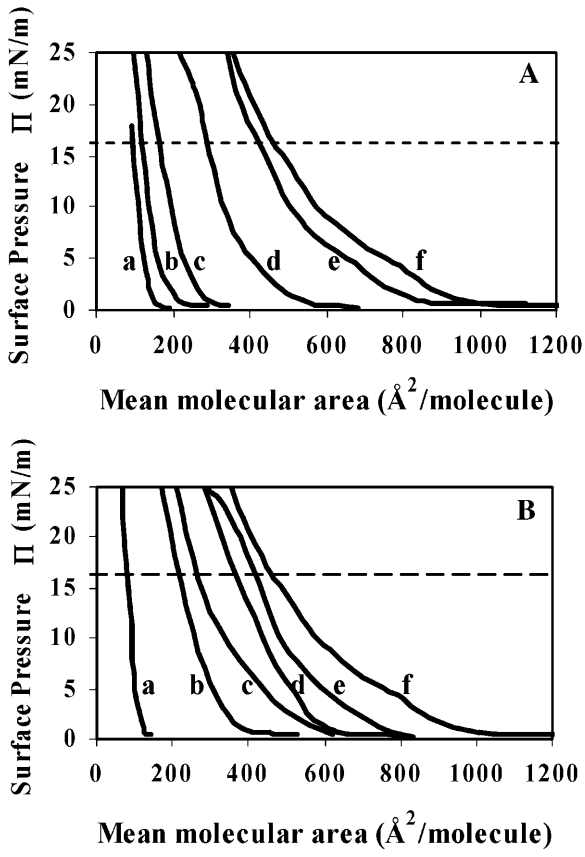

FIGURE 3 Compression isotherms. (*A*) hCT(9–32)/DOPC mixtures. The peptide molar fraction x_{hCT} is (*a*) 0, (*b*) 0.1, (*c*) 0.25, (*d*) 0.5, (*e*) 0.75, and (*f*) 1. The horizontal dashed line leads to the values used in Fig. 4 *A*. The subphase was pure water. (*B*) hCT(9–32)/DOPG mixtures. The peptide molar fraction x_{hCT} is (*a*) 0, (*b*) 0.05, (*c*) 0.1, (*d*) 0.25, (*e*) 0.5, (*e*) 0.75, and (*g*) 1. The horizontal dashed line leads to the values used in Fig. 4 *B*. The subphase was pure water.

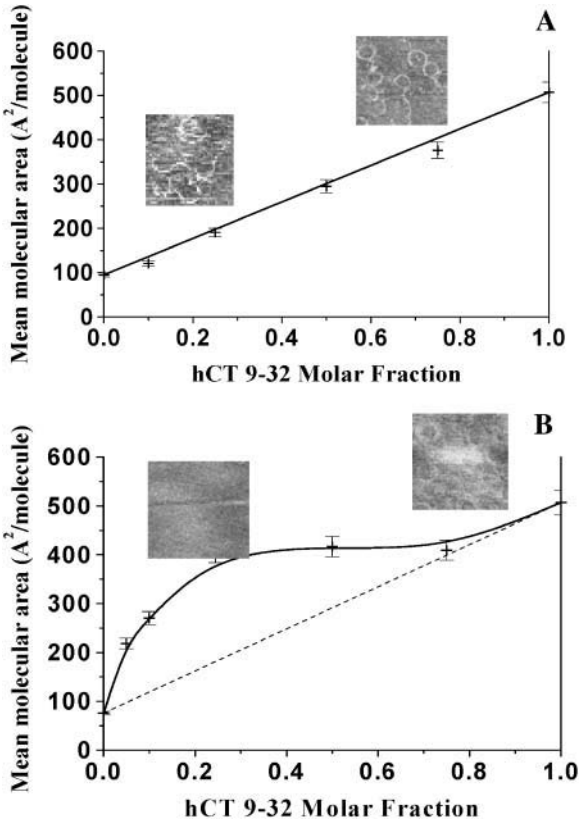

FIGURE 4 Variation of the mean molecular area at 16 mN/m as a function of the hCT(9–32) molar fraction when mixed with (*A*) DOPC (data were obtained from Fig. 3 *A*) and (*B*) DOPG (data were obtained from Fig. 3 *B*). (*Insets*) AFM images correspond to the 0.1 (*left*) and 0.5 (*right*) molar fractions.

Fig. 4 *A*, which corresponds to the behavior of hCT(9–32) in the presence of DOPC, reveals a linear variation of the mean molecular area with the peptide molar fraction. In the case of DOPG, a positive deviation occurs in the peptide molar fraction range of 0–0.75 (Fig. 4 *B*). These two figures show that, whereas hCT(9–32) does not interact with DOPC, it presumably interacts strongly with DOPG with an expansion of the mean molecular area arising probably from repulsive interactions between negative charges (D15 and the headgroups) and/or reorganization of the peptide molecules. This expansion holds true, at least, up to the peptide molar fraction of 0.75; above this value, DOPG and hCT(9–32) are not miscible (Gaines, 1966). All these results were confirmed by the AFM observations (see below). The behavior detected in the presence of DOPG is in accordance with those reported by Epand et al. (1983), who have shown that full-length hCT is able to solubilize DMPG vesicles, whereas only moderate or no interactions could be detected with several other phospholipids. Similarly, Stipani et al. (2001) underlined the importance of the addition of 15% DOPG in lipid bilayers for the detection of hCT channel activity.

Conformation of the hCT(9–32) fragment

In solution

When in solution in pure water, the CD spectrum of hCT(9–32) is characterized by the presence of a single negative band at 199 nm identifying a nonordered structure (Fig. 5 *A*). The ability for this peptide to adopt an α-helical structure was checked by successive additions of sodium dodecylsulfate (SDS) up to the CMC of the detergent. Below this CMC, the presence of SDS does not induce significant folding of the peptide, whereas a partial α-helical folding occurs when the CMC of SDS is reached as already described earlier by others (Epand et al., 1983, 1985; Motta et al., 1991). Such a behavior is in full agreement with the structural analyses reported previously on full-length calcitonin (Epand et al., 1983, 1985; Siligardi et al., 1994; Motta et al., 1998).

At interfaces

To approach membrane-like conditions, monolayers constituted of either pure peptide or peptide-lipid mixtures at a peptide molar fraction of 0.38 were transferred by the Langmuir-Blodgett method onto quartz slides at a surface pressure of 20 mN/m. All spectra (Fig. 5 *B*) indicate an α-helical conformation in the presence and absence of lipids, as characterized by the existence of a positive band

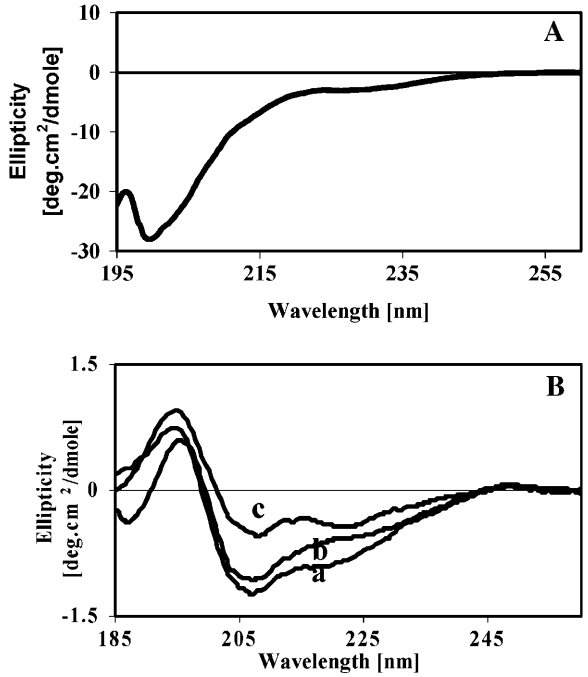

FIGURE 5 Circular dichroism spectra of hCT(9–32) in various conditions. (*A*) In aqueous solution (c = 0.2 mg/mL). (*B*) Monolayers containing hCT(9–32) transferred onto quartz plates by the Langmuir-Blodgett method: (*a*) without lipids, (*b*) in the presence of DOPG, and (*c*) in the presence of DOPC.

at 195 nm accompanied by a minimum at 207 nm in association with another band or a shoulder ~222 nm (Greenfield and Fasman, 1969; Briggs et al., 1986). These measurements could not be quantified because the real peptide concentration used is unknown. Nevertheless, the shape of the spectra and particularly the relative intensities of the 195 and 207 nm bands for the pure peptide suggest a fully helical structure.

To access the conformational state of hCT(9–32) at interfaces, FTIR spectra of peptide-containing multilayers at the solid-air interface were recorded. The spectrum detected for pure peptide is almost identical to those obtained for peptide-lipid mixtures (Fig. 6). The spectral characteristics are independent of the peptide/lipid ratio and the nature of the phospholipid headgroups. All spectra clearly reveal the existence of a broad amide I band centered at ~1660 cm^{-1}. Wavenumbers of the amide I band in this region are indicative of the presence of an α-helical conformation. The existence of a nonordered structure contribution cannot be ruled out (Arrondo and Goni, 1999). Further, the absence of any contribution in the 1630 cm^{-1} region (no shoulder can be detected even by the second derivative approach) indicates that the peptide has little tendency to adopt an antiparallel β-sheet structure, at least in the presence of phospholipids. Only a slight broadening of the amide I band toward higher wavenumbers of ~1670 cm^{-1} could account for the existence of β-turns in the presence of lipids. The shape and positions of the amide II band are in line with the above assignments.

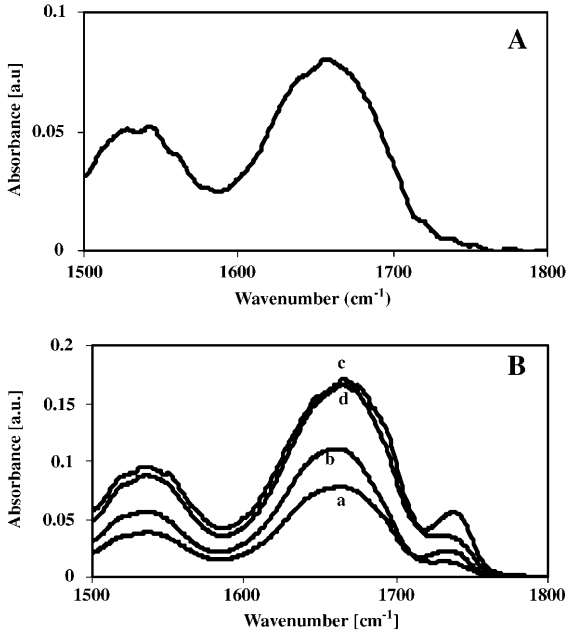

FIGURE 6 FTIR spectra of hCT(9–32)-containing multilayers in absence and presence of phospholipids. (*A*) Pure hCT(9–32). (*B*) (*a*) hCT(9–32)/DOPC 1:3 (mol/mol), (*b*) hCT(9–32) DOPC 1:1 (mol/mol), (*c*) hCT(9–32)/DOPG 1:3 (mol/mol), and (*d*) hCT(9–32)/DOPG 1:1 (mol/mol).

AFM observations on LB transfers

The AFM observations were performed on LB films transferred at a surface pressure of 20 mN/m onto a cleaved mica surface. The images obtained on pure monolayers of lipid, i.e., DOPC and DOPG, exhibit, as expected, a clean and flat surface without any particular structure (Fig. 7, *A* and *B*). On the other hand, a particular supramolecular structure protruding from the matrix, which looks like filaments rolled into spirals, was observed on pure hCT(9–32) monolayers (Fig. 7 *C*). The structure is more visible in Fig. 7, *D* and *E*, which are zooms of Fig. 7 *C*.

The filaments are regularly deposited on the surface of the sample and protrude from the matrix by ~1 nm. They are very close to each other but do not overlap. Representative

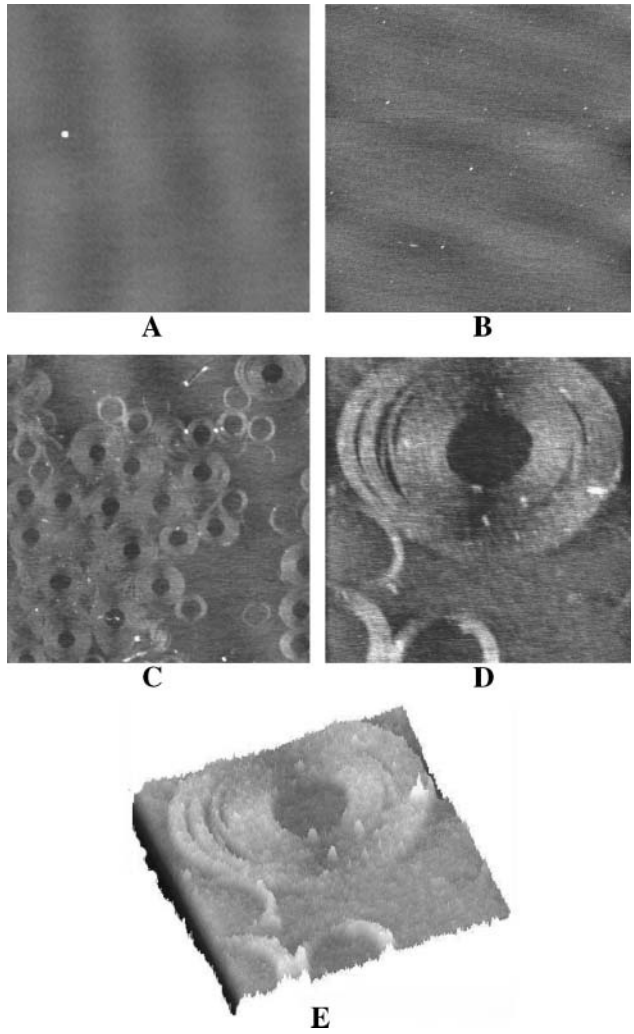

FIGURE 7 AFM imaging of pure compound LB monolayers. The transfers were carried out at 20 mN/m and examined in air, using contact mode. (*A*) Monolayer of pure DOPC; scan size 5 μm × 5 μm. (*B*) Monolayer of pure DOPG; scan size 5 μm × 5 μm. (*C*) Monolayer of pure hCT(9–32); scan size 5 μm × 5 μm. (*D*) Enlargement of *C* with a scan size of 1.2 μm × 1.2 μm. (*E*) Three-dimensional representation of *D*.

images of the mica-supported DOPC/hCT(9–32) LB films at different peptide molar fractions (x_{hCT}) from 0.1 to 0.5 are shown in Fig. 8. Whatever the peptide molar fraction, we observe the presence of the characteristic spiral structure; the number of structures increases with the peptide concentration (see Fig. 8, *A* and *D*). These results, which indicate that the structure adopted by the peptide at the air-water interface is not markedly modified by the presence of DOPC, are in good agreement with the findings of the isotherm compression analysis.

Replacing the zwitterionic phosphatidylcholine headgroup, which is electrically neutral at physiological pH, by the negatively charged phosphatidylglycerol does not alter the spiral structures of hCT(9–32) for $x_{hCT} > 0.5$ (Fig. 9, *B–D*). High-resolution imaging of the $x_{hCT} = 0.5$ provides further details about the structural organization of the calcitonin fragment (Fig. 9, *C* and *D*). This circular structure is open and has a diameter of 14 nm. On the other hand, in contrast to DOPC, for low peptide molar fractions below 0.5, the surface of the monolayers was flat and homogeneous (Fig. 9 *A*) and we did not observe any circular structure. It is worth noting that for this range of concentration, the isotherm compression analysis indicates the existence of strong interactions between hCT(9–32) and DOPG. Since these supramolecular peptide structures do not occur when the peptide interacts with lipids, it can be suggested that the peptide-lipid interactions induce a modification of the organization of hCT(9–32) at the air-water interface.

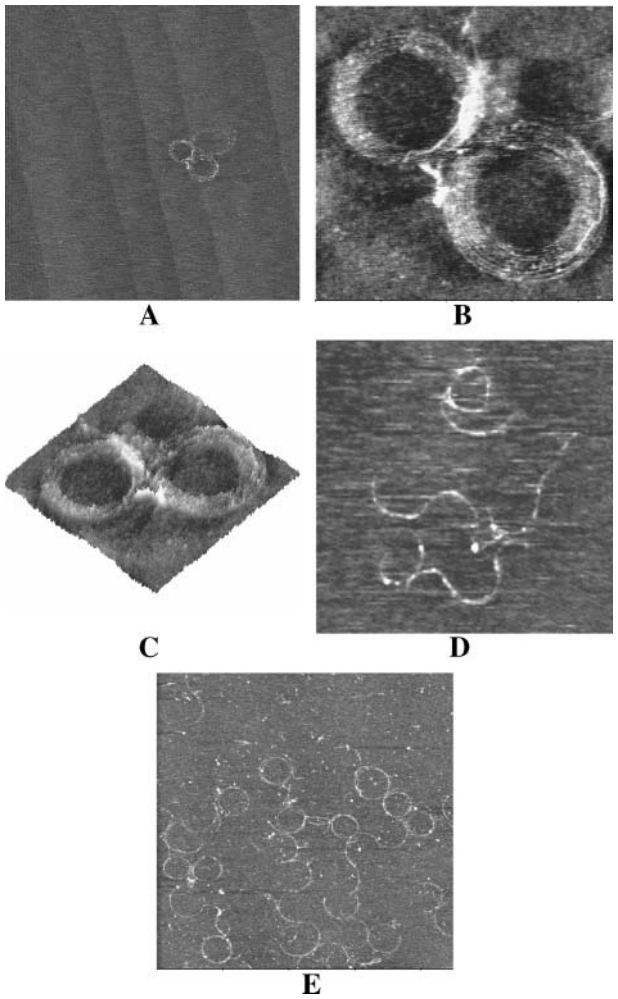

FIGURE 8 AFM imaging of DOPC/hCT(9–32) LB monolayers. (*A*) $x_{hCT} = 0.1$; scan size 5 μm × 5 μm. (*B*) Zoom of *A* on a circular shape; scan size 910 nm × 910 nm. (*C*) Three-dimensional representation of *B*. (*D*) $x_{hCT} = 0.5$; scan size 4.5 μm × 4.5 μm. (*E*) $x_{hCT} = 0.5$; scan size 2.5 μm × 2.5 μm. At low concentrations of hCT(9–32), the spiral structure is sometimes open.

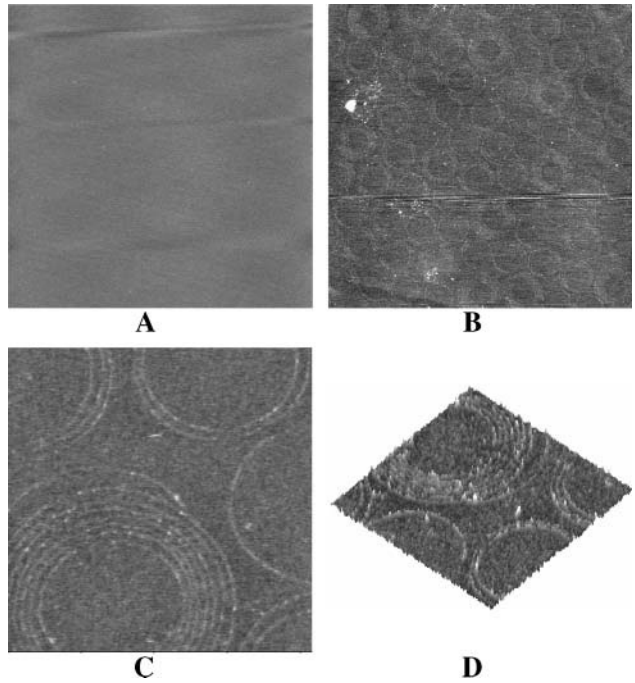

FIGURE 9 AFM imaging of DOPG/hCT(9–32) LB monolayers at various peptide concentrations. Films were transferred at 20 mN/m and examined in air using contact mode. (*A*) $x_{hCT} = 0.1$; scan size 5 μm × 5 μm. (*B*) $x_{hCT} = 0.5$; scan size 5 μm × 5 μm. (*C*) Zoom of *B* on an open circular shape; scan size 833 nm × 833 nm. (*D*) Three-dimensional representation of *C*.

A molecular model of the spiral structure formed by hCT(9–32)

Several assumptions are needed to construct a model of hCT(9–32), whose sequence is L^{9}GTYTQDF^{16}NKFHT-FP^{23}QTAIGVGAP^{32}-NH_2. The main one is that the peptide hCT(9–32) adopts the α-helical conformation. Although this assumption appears to conflict with structural models of full-length hCT, which contain a β-sheet structure (Schmidt et al., 1998; Kamihira et al., 2000) it is strongly supported by our CD (Fig. 5) and FTIR (Fig. 6) observations, especially the fact that no β-sheet contribution could be detected. In addition, the finding of strong interactions with DOPG

(Fig. 4 *B*) indicates the existence of a hydrogen bonding pattern that very probably concerns the whole peptide: Otherwise miscibility would not occur for energetic reasons (Ladokhin and White, 1999). Finally, the spectroscopic data (Figs. 5 and 6) favor the existence of a helical structure. Assuming that the helical axis is oriented parallel to the air-water interface, its calculated dimensions ($\sim$1.5 Å helix pitch $\times$ $24_{\text{number of residues}} \times 13$ $\text{Å}_{\text{helix diameter}} = 468$ Å^2) are consistent with the molecular area measured by the compression isotherms of pure hCT(9–32) (Fig. 3 *A*, trace *f*).

Our molecular model also rests upon the assumption that, at the air-water interface, hydrophobic (or apolar) patches of the amphipathic hCT(9–32) α-helices face the air, whereas hydrophilic areas are directed toward the water. Our molecular modeling and energy minimization of the hCT(9–32) α-helix show that Pro^{23} slightly bends the helix at a position that is located two-thirds away from the N-terminus (see *arrow* in Fig. 10 *A*). The helix bends in such a way that it remains within the air-water plane if its hydrophobic surface is directed toward air and the hydrophilic one toward water. It is worth mentioning that during the energy minimization, hCT(9–32) retains its α-helical structure, except the last C-terminal residue Pro^{32}. The stereochemical analysis of the hCT(9–32) α-helix indicates that the hydrophobic surface is sufficiently wide to provide part of its apolar side chains, mainly the Phe residues in positions 16, 19, and 22, for side-by-side interactions of the helices within the air-water interface. The in-register arrangement of the N-terminal parts of the α-helices is suggested because it allows the most favorable knob-in-hole packing of the side chains between the helices. This arrangement is also favorable for polar and charged side chains such as the negatively charged Asp^{15} and the positively charged Lys^{18} that are present on the hydrophobic surface. Indeed, these residues are aligned on the hydrophobic side (Fig. 10, *B* and *C*) and could form favorable electrostatic interactions due to their alternation. In addition, Thr^{11} and Tyr^{12} can form an interhelical hydrogen bond. The formation of Asp^{15}-Lys^{18} ionic bonds and Thr^{11}-Tyr^{12} hydrogen bonds should also decrease the energy spending that is associated with the water-to-air transfer of these residues. Such energetically unfavorable location of these polar and charged residues can be explained by compensatory hydrophobic interactions of the remaining apolar residues. Our estimation suggests that this arrangement will be more favorable than the alternative one with a loss of $\sim$10 hydrogen bonds at the hydrophilic side of the helix. Interestingly, the side-by-side packing of the C-terminal third of the α-helices do not have a knob-in-hole fit due to the Pro^{23}-originated bend (Fig. 10). As a result, the energy minimization of the layer of hCT(9–32) α-helices increases the interhelical distance of the C-terminus (1.20 nm) compared to the N-terminus (1.17 nm). This difference in the interhelical distances causes a curvature of the α-helical layers with a diameter of $\sim$300 nm (Fig. 10) that is in a good agreement with the observed curvature of the spirals with a diameter of 300–400 nm. In accordance with our structural model, the observed preferable range of the spiral diameters is controlled by the allowed range of 0.01nm of the N-C distance differences of the hCT(9–32) packing. The dimensions of the spiral suggest that several α-helical layers may interact with each other by their N-terminal and C-terminal edges. The formation of the spiral can be explained by the fast propagation of the hCT(9–32) association in the direction of side-by-side packing compared to their

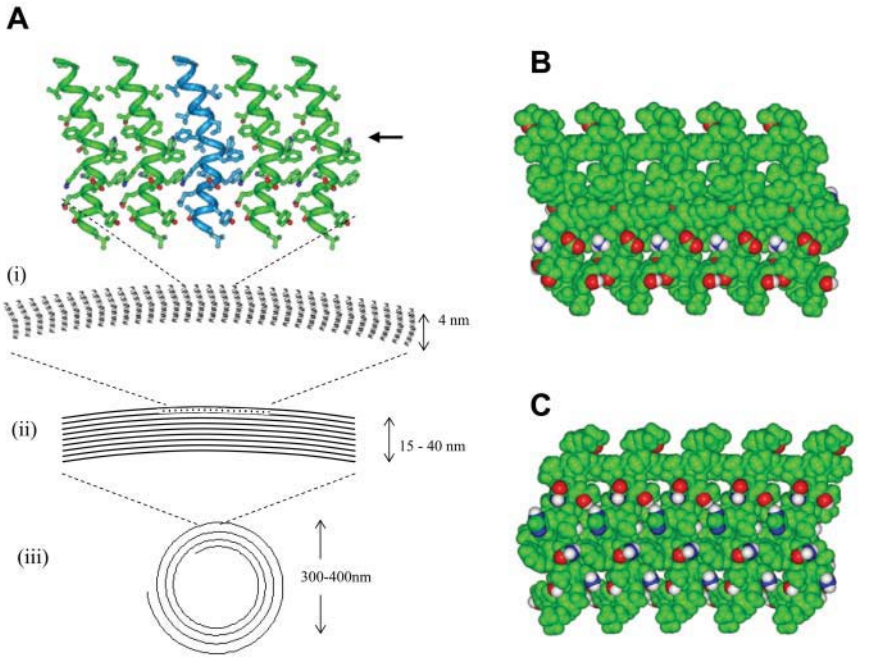

FIGURE 10 Structural model of the peptide spiral. (*A*) Schematic representation of different levels of the structural arrangement of the spiral. On the top, an enlarged picture of the side-by-side packing of five α-helices bent at Pro^{23} (*arrow*). The backbone of the α-helix is present as a ribbon, whereas side chains are shown by ball-and-stick representation. Ribbons and carbon atoms of four helices are in green, and one helix is outlined by light blue. Oxygen atoms are in red and nitrogen atoms are in blue. Below, the diagrams show (*i*) a layer formed by association of such α-helices; (*ii*) a fragment of the spiral formed by several layers; and finally (*iii*) the spiral. (*B*) Hydrophobic surface of the fragment of the layer formed by five α-helices (the same as on *A*, *top*). The apolar surface is shown by green. Oxygen, nitrogen, and hydrogen atoms of polar and charged side chains are in red, blue, and white, respectively. (*C*) Opposite hydrophilic surface of the layer.

head-to-tail growth. The first layer serves as a nucleus for subsequent association of the α-helices to form a multilayer ribbon. The merger of adjacent ribbons can be hampered by absence of the fit between their edges.

CONCLUSION

This study confirms that the hCT(9–32) peptide possesses an amphipathic character and has a CMC of $2.5.10^{-7}$ Mole/L (Fig. 1). Measurements of the critical pressure of insertion (Fig. 2) revealed that a spontaneous insertion of hCT(9–32) into lipid bilayers would require a peptide concentration higher than the CMC. Subsequently, this physicochemical study clearly excludes the penetration of membranes as the mechanism of translocation, but instead represents another indication for an endocytic internalization pathway as proposed based on in vivo studies (Schmidt et al., 1998). Compression isotherms of mixed monolayers (Fig. 3), preformed by cospreading hCT(9–32) and DOPG, showed an expansion of the mean molecular area due to an interaction of both components. This interaction of hCT(9–32) was uniquely detected with DOPG and not with zwitterionic DOPC (Fig. 4). The compression isotherms are consistent with our AFM observations that revealed a unique phase for mixed monolayers of interacting hCT(9–32) and DOPG (Figs. 7–9), but showed two immiscible phases for the peptide and DOPC. The expansion resulting from this selective interaction of hCT(9–32) with negatively charged phospholipids could lead to a modification of the membrane that might be of importance for the process of internalization of the peptide into the cell. However, it needs to be considered that this peptide-lipid interaction might not be sufficient for an efficient transfer by an endocytic mechanism. The cellular uptake of hCT(9–32) could therefore require other membrane components than lipids.

CD measurements in solution revealed a random coil conformation of hCT(9–32). At interfaces, CD and FTIR spectroscopies (Figs. 5 and 6) detected a transformation of the peptide into an α-helical structure in the absence and presence of zwitterionic or negatively charged phospholipids. AFM images of the LB films consisting of hCT(9–32) alone or mixed with DOPC showed the formation of a particular supramolecular structure. The peptide tends to be organized in filaments rolled into spirals; according to the spectroscopic results these spiral-like filaments are composed of α-helices (Fig. 10). They differ from the previously described straight fibrils of the full-length calcitonin that consist of both α-helical and β-sheet secondary structure components (Arvinte et al., 1993; Kamihira et al., 2000). A model of the association of hCT(9–32) into this filamentous structure is proposed to account for the AFM observations. Since the formation of filamentous spirals by hCT(9–32) could not be detected when the peptide interacted with DOPG, it is not clear whether the ability to self-assemble plays a role in the hCT(9–32) translocation across the membrane and thus, leads to a cell-penetrating function. This question requires further investigation. Finally, it is worth mentioning that unusual architecture of this structure makes it an attractive template for the bioengineering of different spiral-like associates.

Our thanks are due to Dr. T. Barman for his help in correcting the English.

This work was supported by European Union grant QLK2-2001-01451.

REFERENCES

Adamson, A. W. 1990. Physical Chemistry of Surfaces, 5th ed. Wiley Interscience, New York.

Arrondo, J. L., and F. M. Goni. 1999. Structure and dynamics of membrane proteins as studied by infrared spectroscopy. *Prog. Biophys. Mol. Biol.* 72:367–405.

Arvinte, T., A. Cudd, and A. F. Drake. 1993. The structure and mechanism of formation of human calcitonin fibrils. *J. Biol. Chem.* 268:6415–6422.

Briggs, M. S., D. G. Cornell, R. A. Dluhy, and L. M. Gierasch. 1986. Conformations of signal peptides induced by lipids suggest initial steps in protein export. *Science.* 233:206–208.

Brockman, H. 1999. Lipid monolayers: why use half a membrane to characterize protein-membrane interactions? *Curr. Opin. Struct. Biol.* 9:438–443.

Colman, E., R. Hedin, J. Swann, and D. Orloff. 2002. A brief history of calcitonin. *Lancet.* 359:885–886.

Dauber-Osguthorpe, P., V. A. Roberts, D. J. Osguthorpe, J. Wolff, M. Genest, and A. T. Hagler. 1988. Structure and energetics of ligand binding to proteins: *Escherichia coli* dihydrofolate reductase-trimethoprim, a drug-receptor system. *Proteins.* 4:31–47.

Dayring, H. E., A. Tramonato, S. R. Sprang, and R. J. Fletterick. 1986. Interactive program for visualization and modeling of proteins, nucleic acids and small molecules. *J. Mol. Graph.* 4:82–87.

Demel, R. A., W. S. Geurts van Kessel, R. F. Zwaal, B. Roelofsen, and L. L. VanDeenen. 1975. Relation between various phospholipase actions on human red cell membranes and the interfacial phospholipid pressure in monolayers. *Biochim. Biophys. Acta.* 406:97–107.

Epand, R. M., R. F. Epand, R. C. Orlowski, R. J. Schlueter, L. T. Boni, and S. W. Hui. 1983. Amphipathic helix and its relationship to the interaction of calcitonin with phospholipids. *Biochemistry.* 22:5074–5084.

Epand, R. M., R. F. Epand, and R. C. Orlowski. 1985. Presence of an amphipathic helical segment and its relationship to biological potency of calcitonin analogs. *Int. J. Pept. Protein Res.* 25:105–111.

Gaines, G. L. 1966. Mixed monolayers. *In* Insoluble Monolayers at Liquid-Gas Interfaces. I. Prigogine, editor. Wiley Interscience, New York. 281–300.

Greenfield, N., and G. D. Fasman. 1969. Computed circular dichroism spectra for the evaluation of protein conformation. *Biochemistry.* 8: 4108–4116.

Kamihira, M., A. Naito, S. Tuzi, A. Y. Nosaka, and H. Saito. 2000. Conformational transitions and fibrillation mechanism of human calcitonin as studied by high-resolution solid-state ^{13}C NMR. *Protein Sci.* 9:867–877.

Ladokhin, A. S., and S. H. White. 1999. Folding of amphipathic alpha-helices on membranes: energetics of helix formation by melittin. *J. Mol. Biol.* 285:1363–1369.

Laskowski, R. A., M. W. McArthur, D. S. Moss, and J. M. Thornton. 1993. PROCHECK: a program to check the stereochemical quality of protein structures. *J. Appl. Crystallogr.* 26:282–291.

Law, S. L., and C. L. Shih. 1999. Adsorption of calcitonin to glass. *Drug Dev. Ind. Pharm.* 25:253–256.

Machova, Z., C. Mühle, U. Krauss, R. Tréhin, A. Koch, H. P. Merkle, and A. G. Beck-Sickinger. 2002. Cellular internalization of enhanced green

fluorescent protein ligated to a human calcitonin-based carrier peptide. *Chembiochem.* 3:672–677.

Maget-Dana, R., D. Lelievre, and A. Brack. 1999. Surface active properties of amphiphilic sequential isopeptides: comparison between alpha-helical and beta-sheet conformations. *Biopolymers.* 49:415–423.

Motta, A., G. Andreotti, P. Amodeo, G. Strazzullo, and M. A. Castiglione-Morelli. 1998. Solution structure of human calcitonin in membrane-mimetic environment: the role of the amphipathic helix. *Proteins.* 32: 314–323.

Motta, A., A. Pastore, N. A. Goud, and M. A. Castiglione-Morelli. 1991. Solution conformation of salmon calcitonin in sodium dodecyl sulfate micelles as determined by two-dimensional NMR and distance geometry calculations. *Biochemistry.* 30:10444–10450.

Nakamuta, H., Y. Itokazu, M. Koida, R. C. Orlowski, and R. M. Epand. 1991. Autoradiographic localization of human calcitonin sensitive binding sites in rat brain. *Jpn. J. Pharmacol.* 56:551–555.

Nakamuta, H., R. C. Orlowski, and R. M. Epand. 1990. Evidence for calcitonin receptor heterogeneity: binding studies with nonhelical analogs. *Endocrinology.* 127:163–168.

Savitsky, A., and M. J. E. Golay. 1964. Smoothing and differentiation of data by simplified least squares procedures. *Anal. Chem.* 36:1627–1639.

Schmidt, M. C., B. Rothen-Rutishauser, B. Rist, A. G. Beck-Sickinger, H. Wunderli-Allenspach, W. Rubas, W. Sadée, and H. P. Merkle. 1998. Translocation of human calcitonin in respiratory nasal epithelium is associated with self-assembly in lipid membrane. *Biochemistry.* 37: 16582–16590.

Siligardi, G., B. Samori, S. Melandri, M. Visconti, and A. F. Drake. 1994. Correlations between biological activities and conformational properties for human, salmon, eel, porcine calcitonins and elcatonin elucidated by CD spectroscopy. *Eur. J. Biochem.* 221:1117–1125.

Silverman, S. L. 1997. Calcitonin. *Am. J. Med. Sci.* 313:13–16.

Stipani, V., E. Gallucci, S. Micelli, V. Picciarelli, and R. Benz. 2001. Channel formation by salmon and human calcitonin in black lipid membranes. *Biophys. J.* 81:3332–3338.

Stroop, S. D., H. Nakamuta, R. E. Kuestner, E. E. Moore, and R. M. Epand. 1996. Determinants for calcitonin analog interaction with the calcitonin receptor N-terminus and transmembrane-loop regions. *Endocrinology.* 137:4752–4756.

Van Mau, N., V. Vié, L. Chaloin, E. Lesniewska, F. Heitz, and C. Le Grimellec. 1999. Lipid-induced organization of a primary amphipathic peptide: a coupled AFM-monolayer study. *J. Membr. Biol.* 167:241–249.

Vié, V., N. Van Mau, L. Chaloin, E. Lesniewska, C. Le Grimellec, and F. Heitz. 2000. Detection of peptide-lipid interactions in mixed monolayers, using isotherms, atomic force microscopy, and Fourier transform infrared analyses. *Biophys. J.* 78:846–856.

Yoshikawa, S., K. Shinzawa-Itoh, R. Nakashima, R. Yaono, E. Yamashita, N. Inoue, M. Yao, M. J. Fei, C. P. Libeu, T. Mizushima, H. Yamaguchi, T. Tomizaki, and T. Tsukihara. 1998. Redox-coupled crystal structural changes in bovine heart cytochrome c oxidase. *Science.* 280:1723–1729.